
Non-Markovian Reward Modelling from Trajectory Labels via Interpretable Multiple Instance Learning

Joseph Early ^{*‡}Tom Bewley ^{†‡}Christine Evers ^{*}Sarvapali Ramchurn ^{*‡}

Abstract

We generalise the problem of reward modelling (RM) for reinforcement learning (RL) to handle non-Markovian rewards. Existing work assumes that human evaluators observe each step in a trajectory independently when providing feedback on agent behaviour. In this work, we remove this assumption, extending RM to include hidden state information that captures temporal dependencies in human assessment of trajectories. We then show how RM can be approached as a multiple instance learning (MIL) problem, and develop new MIL models that are able to capture the time dependencies in labelled trajectories. We demonstrate on a range of RL tasks that our novel MIL models can reconstruct reward functions to a high level of accuracy, and that they provide interpretable learnt hidden information that can be used to train high-performing agent policies.

1 Introduction

There is growing consensus around the view that aligned and beneficial AI requires a reframing of objectives as being contingent, uncertain, and learnable via interaction with humans [31]. In reinforcement learning (RL), this proposal has found one formalisation in reward modelling (RM): the inference of agent objectives from human preference information such as demonstrations, pairwise choices, approval labels, and corrections [25]. Prior work in RM typically assumes that a human evaluates the *return* (quality) of a sequential trajectory of agent behaviour by summing equal and independent *reward* assessments of instantaneous states and actions, with the aim of RM being to reconstruct the underlying reward function. However, in reality the human’s experience of a trajectory is likely to be temporally-extended (e.g., via a video clip [12] or real-time observation), which opens the door to dependencies between earlier events and the assessment of later ones. The independence assumption may be both psychologically unrealistic given human memory limitations [23], and technically naïve given the difficulty of building complete instantaneous state representations [22]. We thus seek to generalise RM to allow for temporal dependencies in human evaluation, by postulating *hidden state* information that accumulates over a trajectory. Reconstruction of the human’s preferences now requires the modelling of hidden state dynamics alongside the reward function itself.

In tackling this generalised problem, we identify a structural isomorphism between RM (specifically from trajectory return labels) and the established field of multiple instance learning (MIL) [10]. Trajectories are recast as *bags* and constituent state-action pairs as *instances*, which collectively contribute to labels provided at the bag level by interacting in potentially complex ways. This mapping inspires a range of novel MIL model architectures that use long short-term memory (LSTM) modules [16] to recover the hidden state dynamics, and learn instance-level reward predictions from return-labelled trajectories of arbitrary length. In experiments with synthetic oracle labels, we show that our novel MIL RM models can accurately reconstruct ground-truth hidden states and reward functions for non-Markovian tasks, and can be straightforwardly integrated into RL agent training to achieve performance matching, or even exceeding, that of agents with direct access to true hidden states and rewards. All of our source code is available in a public repository.¹

^{*}University of Southampton, United Kingdom; {J.A.Early,C.Evers,sdr1}@soton.ac.uk

[†]University of Bristol, United Kingdom; tom.bewley@bristol.ac.uk

[‡]The Alan Turing Institute, United Kingdom

¹<https://github.com/JAEarly/MIL-for-Non-Markovian-Reward-Modelling>

Our contributions are as follows:

1. We generalise RM to handle *non-Markovian* rewards that depend on hidden features of the environment or the psychology of the human evaluator in addition to visible states/actions.
2. We identify a structural connection between RM and MIL, creating the opportunity to transfer concepts and methods between the two fields.
3. We propose two novel LSTM-based MIL models for this generalised RM problem, and develop interpretability techniques for understanding and verifying the learnt reward functions.
4. We compare our proposed models to existing MIL baselines on four non-Markovian tasks, evaluating return prediction, reward prediction, robustness to label noise, and interpretability.
5. We demonstrate that the hidden state and reward predictions of our MIL RM models can be used by RL agents to solve non-Markovian tasks.

The remainder of this work is as follows. Section 2 discusses related work in RM and MIL, Section 3 gives a formal problem definition and describes our MIL-inspired methodology, and Section 4 presents our experiments and results. We discuss key findings in Section 5, and Section 6 concludes.

2 Background and Related Work

Reward Modelling RM [25] aims to infer a reward function from revealed human preference information such as demonstrations [28], pairwise choices [12], corrections [4], good/bad/neutral labels [29], or combinations thereof [21]. Most prior work assumes a human evaluates a trajectory by summing independent rewards for each state-action pair, but in practice their experience is likely to be temporally-extended (e.g., via a video clip), creating the opportunity for dependencies to emerge between earlier events and the assessment of later ones. As noted by Chan et al. [11] and Bewley and Lecue [8], such dependencies may arise from cognitive biases such as anchoring, prospect bias, and the peak-end rule [23], but they could equally reflect rational drivers of human preferences not captured by the state representation. Some efforts have been made to model temporal dependencies, such as a discrete psychological mode which evolves over consecutive queries about hypothetical trajectories [6], or a monotonic bias towards more recently-viewed timesteps due to human memory limitations [24]. Elsewhere, Shah et al. [32] use human demonstrations and binary approval labels to learn temporally-extended task specifications in logical form. In comparison to these restricted examples, our work provides a more general approach to capturing temporal dependencies in RM.

Non-Markovian Rewards In the canonical RL problem setup of a Markov decision process (MDP), rewards depend only on the most recent state-action pair. In a non-Markovian reward decision process (NMRDP) [2], rewards depend on the full preceding trajectory [2]. NMRDPs can be *expanded* into MDPs (and thus solved by RL) by augmenting the state with a hidden state that captures all reward-relevant historical information, but this is typically not known *a priori*. Data-driven approaches to learning NMRDP expansions [18] often make use of domain-specific propositions and temporal logic operators [3, 35, 37]. Outside of the RM context, recurrent architectures such as LSTMs have been used in NMRDPs to reduce reliance on pre-specified propositions [20]. They also have a long history of use in partially observable MDPs, where dynamics are also non-Markovian [5, 42, 14].

Multiple Instance Learning In MIL [10], datasets are structured as collections of bags $X_i \in \mathbf{X}$, each of which is comprised of instances $\{x_1^i, \dots, x_k^i\}$ and has an associated bag-level label Y_i and instance-level labels $\{y_1^i, \dots, y_k^i\}$. The aim is to construct a model that learns solely from bag labels; instance labels are not available during training, but may be used later to evaluate instance-level predictions. The simplest MIL approaches assume that instances are independent and that the bag is unordered, but models exist for capturing various types of instance dependencies [41, 19, 38]. LSTMs have emerged as a natural architecture for modelling temporal dependencies among ordered bags, where they can be utilised to aggregate instance information into an overall bag representation. They have previously been applied to standard MIL benchmarks [40], as well as specific problems such as Chinese painting image classification [26]. As we discuss in Section 3.2, these existing models are somewhat unsuitable for use in RM, leading us to propose our own novel model architectures.

3 Methodology

In this section, we present the core methodology of our work. We formally define the new paradigm of non-Markovian RM (Section 3.1), before drawing on the MIL literature to propose models that can be used to solve this generalised problem (Section 3.2). We then go on to discuss how we can use our learnt RM models for training RL agents on non-Markovian tasks (Section 3.3).

3.1 Formal Definition of Non-Markovian RM

Consider an agent interacting with an environment with Markovian dynamics. At discrete time t , the current environment state $s_t \in \mathcal{S}$ and agent action $a_t \in \mathcal{A}$ condition the next environment state s_{t+1} according to the dynamics function $D : \mathcal{S} \times \mathcal{A} \rightarrow \Delta\mathcal{S}$. A trajectory $\xi \in \Xi$ is a sequence of state-action pairs, $\xi = ((s_0, a_0), \dots, (s_{T-1}, a_{T-1}))$, and a human's preferences about agent behaviour respect a real-valued return function $G : \Xi \rightarrow \mathbb{R}$. In traditional (Markovian) RM, return is assumed to decompose into a sum of independent rewards over state-action pairs, $G(\xi) = \sum_{t=0}^{T-1} R(s_t, a_t)$, and the aim is to reconstruct $R' \approx R$ from possibly-noisy sources of preference information. In our generalised non-Markovian model, we consider the human to observe a trajectory sequentially and allow for the possibility of hidden state information that accumulates over time and parameterises R :

$$G(\xi) = \sum_{t=0}^{T-1} R(s_t, a_t, h_{t+1}) \quad \text{where} \quad h_{t+1} = \delta(h_t, s_t, a_t), \quad (1)$$

δ is a hidden state dynamics function, and h_0 is a fixed value for the initial hidden state. Reconstruction of the human's preferences now requires the estimation of $\delta' \approx \delta$ and $h'_0 \approx h_0$ alongside $R' \approx R$. We can interpret the hidden information as an external feature of the environment that is visible to the human but excluded from the state, or as a psychological state of the person themselves, through which their response to a new observation is influenced by what they have seen already. Appendix B elaborates on this discussion, presenting motivating use cases and limitations of non-Markovian RM. We visualise the difference between Markovian and non-Markovian RM in Figure 1.

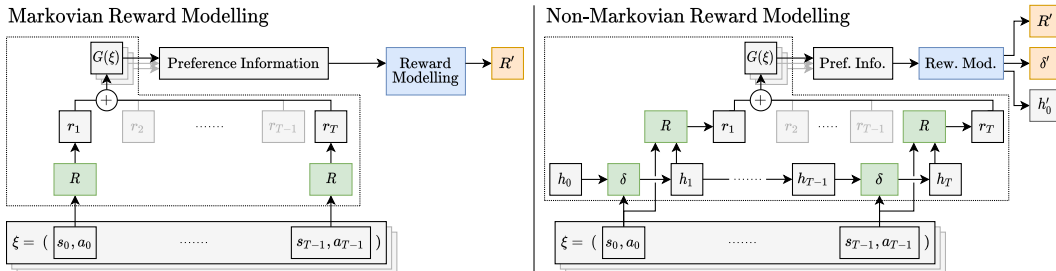


Figure 1: In Markovian RM, the human is assumed to sum over independent and equal assessments of the state-action pairs in a trajectory. In non-Markovian RM, per-timestep rewards additionally depend on hidden state information h that accumulates over time.

In this work, we focus on the simplest and most explicit form of preference information: direct labelling of returns $G(\xi_i)$ for a dataset of N trajectories $\{\xi_i\}_{i=1}^N$. We aim to solve the reconstruction problem by minimising the squared error in predicted returns:

$$\operatorname{argmin}_{R', \delta', h'_0} \sum_{i=1}^N \left(G(\xi_i) - \sum_{t=0}^{T_i-1} R'(s_{i,t}, a_{i,t}, h'_{i,t+1}) \right)^2 \quad \text{where} \quad \begin{aligned} h'_{i,0} &= h'_0 \\ h'_{i,t+1} &= \delta'(h'_{i,t}, s_{i,t}, a_{i,t}) \quad \forall i \in \{1..N\}. \end{aligned} \quad (2)$$

We observe that Equation 2 perfectly matches the definition of a MIL problem. Each trajectory ξ_i can be considered as an ordered bag of instances $((s_{i,0}, a_{i,0}), \dots, (s_{i,T_i-1}, a_{i,T_i-1}))$ with unobserved instance labels $R(s_{i,t}, a_{i,t}, h_{i,t+1})$, an observed bag label $G(\xi_i) = \sum_{t=0}^{T_i-1} R(s_{i,t}, a_{i,t}, h_{i,t+1})$, and temporal instance interactions via the changing hidden state $h_{i,t}$. This correspondence motivates us to review the space of existing MIL models (specifically those that model temporal dependencies among instances) to provide a starting point for developing our non-Markovian RM approach.

3.2 MIL RM Architectures

The MIL literature contains a variety of architectures for handling temporal instance dependencies, including graph neural networks (GNNs) [38] and transformers [33]. While effective for many problems, such architectures are an unnatural fit to non-Markovian RM as they contain no direct analogue of a hidden state h' carried forward in time, instead handling dependencies via some variant of message-passing between instances. LSTM-based MIL architectures [40, 26] provide a more promising starting point since they explicitly represent both h' (implemented as a continuous-valued vector) and its temporal dynamics function δ' (a particular arrangement of gating functions).

Starting from an existing LSTM-based MIL architecture, we propose two successive extensions as well as a naïve baseline that cannot handle temporal dependencies. All four architectures include a feature extractor (FE) for mapping state-action pairs into feature vectors and a head network (HN) that outputs predictions. These architectures are depicted in Figure 2. Note we use the same nomenclature as [10] and [41]: *embedding space* approaches produce an overall bag representation that is used for prediction, while *instance space* approaches produce predictions for each instance in the bag and then aggregate those predictions to a final bag prediction.

Base Case: Embedding Space LSTM This architecture, proposed by Wang et al. [40], processes all instances in a bag sequentially and uses the final LSTM hidden state as a bag embedding. This is fed into the HN, which predicts the bag label g' (return in the RM context). Although this model can account for temporal dependencies, it does not inherently produce instance predictions (rewards), which require some post hoc analysis to recover. While methods exist for computing instance importance values as a form of interpretability [13], these are not guaranteed to sum to the bag label as stipulated by the reward-return formulation. We propose a new method: at time t , the predicted reward r'_t is calculated by feeding the LSTM hidden state at times $t-1$ and t into the HN to obtain two *partial* bag labels/returns g'_{t-1} and g'_t , and computing the difference of the two, i.e., $r'_t = g'_t - g'_{t-1}$. Note that we define $g'_0 = 0$.

Extension 1: Instance Space LSTM The preceding post hoc computation is rather inelegant and often yields poor reward predictions (see Appendix C and Section 4), likely because rewards are never computed or back-propagated through during learning. This leads us to propose an improved architecture, which is structurally similar but differs in how network outputs are mapped onto RM concepts, and places reward predictions on the back-propagation path. Given the LSTM hidden state at time t , the output of the HN is taken to be the instantaneous reward r'_t rather than the partial return. Rewards are computed sequentially for all timesteps in a trajectory and summed to give the return prediction g' . We thereby obtain a model that both handles temporal dependencies and produces explicitly-learnt reward predictions.

Extension 2: Concatenated Skip Connection (CSC) Instance Space LSTM In both of the preceding architectures, the LSTM hidden state h'_t is the sole input to the HN. This requires h'_t to represent all reward-relevant information from both the true hidden state h_t and the latest state-action pair s_{t-1}, a_{t-1} to achieve good performance. To lighten the load on the LSTM, we further extend the Instance Space LSTM model with a skip connection [15, 17] which concatenates the FE output onto the hidden state before feeding it to the HN. In principle, this should allow the hidden state to solely focus on representing temporal dependencies. As well as improving RM performance compared to an equivalent model without skip connections, we find in Section 5.1 that this modification tends to yield more interpretable and disentangled hidden state representations.

Markovian Baseline: Instance Space Neural Network (NN) To quantify the cost of ignoring temporal dependencies, we also run experiments with a baseline architecture that feeds only the FE output for each state-action pair into the HN, yielding fully-independent reward predictions which are summed to give the return prediction. This independent predict-and-sum architecture has precedence in both MIL, where it is referred to as mi-Net by Wang et al. [41], and in RM, where it embodies the de facto standard Markovian reward assumption [12].

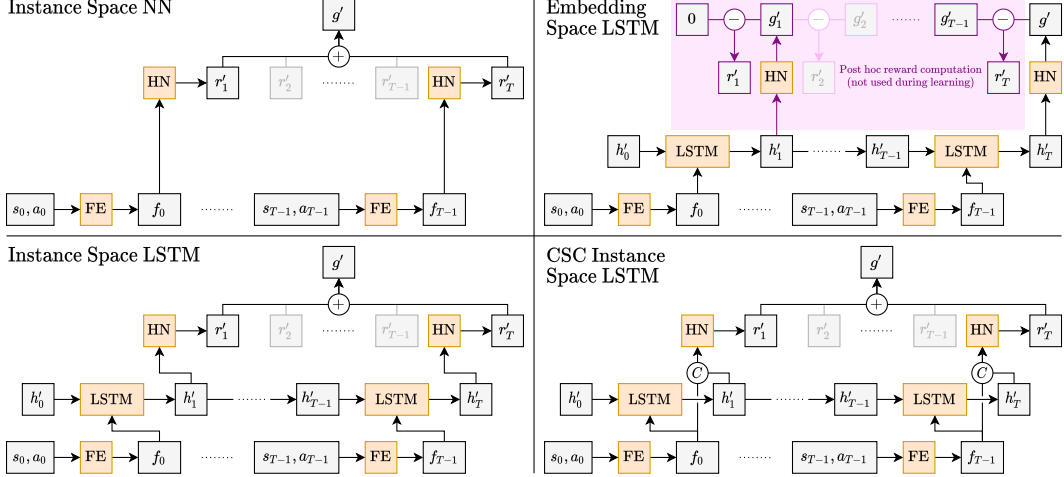


Figure 2: MIL architectures used in this work. FE = feature extractor; HN = head network; $(+)$ = scalar summation; $(-)$ = scalar subtraction; (C) = vector concatenation.

3.3 Training Agents with Non-Markovian RM Models

In this work, as in RM more widely, we are not solely interested in learning reward functions to represent human preferences, but also in the downstream application of rewards to train agents’ action-selection policies. After optimising our LSTM-based models on offline trajectory datasets, we deploy them at the interface between conventional RL agents and their environments. Going beyond prior work, where a learnt model is used to either generate a reward signal for an agent to maximise [12] or augment its observed state representation with hidden state information [18], our models serve a dual role, providing *both* rewards and state augmentations. Figure 3 describes this setup in detail.

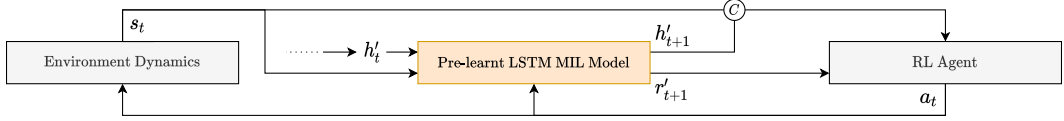


Figure 3: During RL agent training, our LSTM MIL models sit at the centre of the agent-environment loop by which states s_t and actions a_t are exchanged. We focus on episodic tasks, where the environment state periodically resets. The LSTM hidden state is simultaneously reset to h'_0 at the start of an episode, then is iteratively updated over time t given the state-action pairs s_t, a_t . At time t the environment state s_t is augmented with the post-update hidden state h'_{t+1} by concatenation, and this augmented state is observed by the agent. s_t, a_t and h'_{t+1} are used to compute a reward r'_{t+1} following the relevant steps from Figure 2, and the reward is also sent to the agent. In the language of NMRDPs, the hidden state augmentation *expands* the agent’s learning problem into an MDP by providing the additional information required to make the rewards Markovian. Note that unlike during learning of the MIL models, return predictions are never required. Also note the importance of a recurrent model architecture. As they lack a sequentially-updated hidden state, transformer- or GNN-based MIL models would be unsuitable for such online deployment.

4 Experiments and Results

After initially validating our models on several toy datasets (see Appendix C), we focus the bulk of our evaluation on four RL tasks. As running experiments with people is costly, we use the standard RM approach of generating synthetic preference data (here trajectory return labels) using ground-truth *oracle* reward functions [12]. Unlike prior work, these oracle reward functions depend on historical information that cannot be recovered from the instantaneous environmental state, thereby emulating the disparity between the information that a human evaluator possesses while viewing a trajectory sequentially, and that contained in the state alone. In this section, we introduce our RL tasks (Section 4.1), evaluate the quality of reward reconstruction (Section 4.2), investigate the use of MIL RM models for agent training (Section 4.3), and evaluate their robustness to label noise (Section 4.4).

4.1 RL Task Descriptions

We propose four tasks with different types of hidden information. All use a 2D navigation environment with two spawn zones (where the agent initialises), and an episode time limit of $T = 100$; see Figure 4. In each case, the environment state contains the x, y position of the agent only. The tasks involve moving into a *treasure* zone, contingent on some hidden information that cannot be derived from the current x, y position, but is instead a function of the full preceding trajectory. In the first two cases the hidden information varies with time only, but in the other two it depends on the agent’s past positions.

Timer For times $t \leq 50$ the treasure gives a reward of -1 for each timestep that the agent spends inside it, before switching to $+1$ thereafter. Since time is not included in the environment state, recovering the reward function by only observing the agent’s current position is impossible.

Moving The Timer task only captures a binary change, therefore we generalise it to be continuous. In this case, the treasure zone oscillates left and right at a constant speed. Again, this is not captured in the environment state, but can be recovered if the length of the preceding trajectory is known.

Key Before reaching the treasure zone, the agent must first enter a second zone to collect a key; otherwise it receives 0 reward. As the key’s status is not captured in the environment state, a temporal dependency exists between the agent’s past positions and the reward it obtains from the treasure.

Charger We generalise the Key task by replacing the key zone with a charging zone that builds up the amount of reward the agent will receive when it reaches the treasure. Now, the reward is dependent on not only if the agent visits a zone (binary), but how long it is there (continuous).

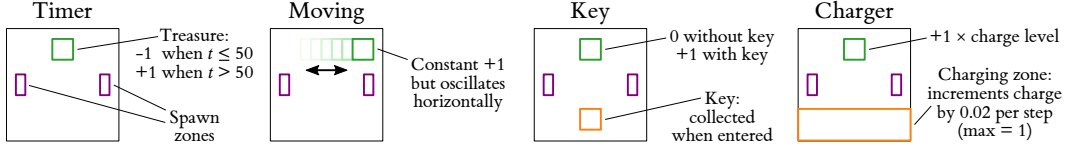


Figure 4: Environment layouts for the four non-Markovian RL tasks.

Further details on the tasks and MIL model hyperparameters are given in Appendix D. One important design decision for the LSTM-based models is the size of the hidden state, as it affects both performance and interpretability. For all the above tasks, we know *a priori* that it is possible to capture the temporal dependencies in at most two dimensions, therefore we constrain our models to use 2D hidden states. This allows us to visualise and interpret the hidden representations in Section 5.1.

4.2 Reward Modelling Results

Below we discuss the performance of the reward reconstruction for the different MIL RM models on our four RL tasks. For each task, we generate 5000 trajectories of length 100 by deploying a random agent and post-screening to obtain a wide distribution of outcomes and return values (see Appendix D for details on the screening process). Summary results from MIL models trained on these trajectories are given in Table 1. We observe the CSC Instance Space LSTM is on average the best performing model for predicting both trajectory returns and timestep rewards. While the Embedding Space LSTM model performs best at predicting return on the Key task, it struggles on the reward metric (as it relies on the use of a proxy post hoc method). Also note that the Instance Space NN that serves as our Markovian RM baseline performs very poorly on return prediction, indicating that these tasks indeed cannot be learnt without modelling temporal dependencies.

Table 1: RL dataset return (top) and reward (bottom) results. Each measurement is the mean MSE averaged over ten repeats, with the standard errors of the mean also given.

Model	Timer	Moving	Key	Charger	Overall
Instance Space NN	130.8 ± 1.530	22.24 ± 0.441	7.764 ± 0.232	7.783 ± 0.214	42.13
Embedding Space LSTM	3.151 ± 0.662	13.04 ± 0.899	0.360 ± 0.055	0.689 ± 0.124	4.311
Instance Space LSTM	7.313 ± 2.627	11.13 ± 1.169	0.488 ± 0.062	0.628 ± 0.126	4.890
CSC Instance Space LSTM	0.605 ± 0.166	5.307 ± 0.299	0.391 ± 0.083	0.125 ± 0.012	1.607
Instance Space NN	0.217 ± 0.001	0.068 ± 0.000	0.011 ± 0.000	0.025 ± 0.000	0.080
Embedding Space LSTM	101.8 ± 60.35	3.033 ± 0.715	0.010 ± 0.008	0.037 ± 0.016	26.23
Instance Space LSTM	0.263 ± 0.038	0.069 ± 0.005	0.002 ± 0.000	0.005 ± 0.001	0.085
CSC Instance Space LSTM	0.073 ± 0.016	0.026 ± 0.002	0.001 ± 0.000	0.001 ± 0.000	0.025

4.3 RL Training Results

Following the method from Section 3.3, we then experiment with training Deep Q-Network (DQN) [27] RL agents to optimise the rewards learnt by the LSTM-based models. We evaluate agent performance in a post hoc manner by passing its trajectories to the relevant oracle. Such an evaluation provides an end-to-end measure of both reward reconstruction and policy learning, and is standard in RM [12]. We baseline against agents trained with access to: a) the oracle reward function and the oracle hidden states, and b) just the oracle reward function without hidden states (i.e, using only the environment states that are missing information). From the results in Figure 5, we observe that the CSC Instance Space LSTM approach leads to the best RL agent performance, coming closest to the oracle. Interestingly, for the Timer task, both the CSC Instance Space LSTM and the Instance Space LSTM actually outperform the use of the oracle, suggesting that the learnt hidden states are easier to exploit for policy learning than the raw timer state (we investigate what these models have learnt in Section 5.1). Note the very poor performance of agents trained without hidden state information, which aligns with expectations. For further details on agent training, see Appendix E.

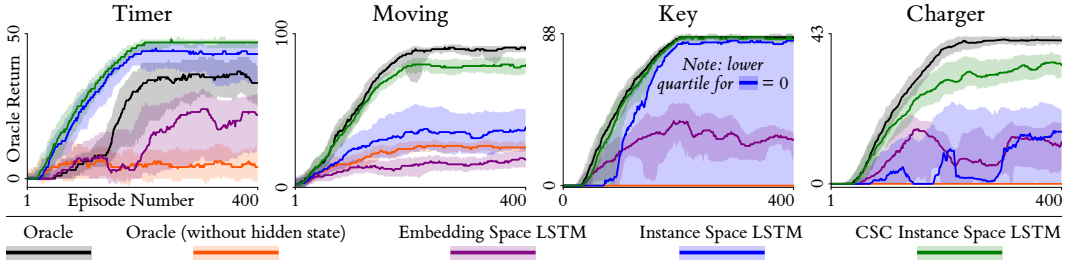


Figure 5: RL performance for different training configurations on our four RL tasks. The results given are the medians and interquartile ranges. For the oracle results, we trained ten repeats, and for the MIL-LSTM results, we performed one RL training run for each MIL-LSTM model repeat.

4.4 Robustness to Mislabelling

In this work, the return labels are provided by oracles rather than real people. When using human evaluators, there are likely to be imperfections and inconsistencies in the labels provided, and it is important to evaluate model robustness against such noise [24]. We implement noise through label swapping [30]; this ensures the marginal label distribution remains the same and does not include out-of-distribution returns. In Figure 6, we show how both return and reward prediction decay with noise levels increasing from 0 (no labels swapped) to 0.5 (half swapped). The rate, smoothness, and consistency (across three repeats) of this decay varies between tasks, with decays in return prediction generally being smoother. We observe that the CSC Instance Space LSTM model remains the strongest predictor of both return and reward in the majority of cases, indicating a general robustness and providing evidence that the model should still be effective with imperfect human labels. On all

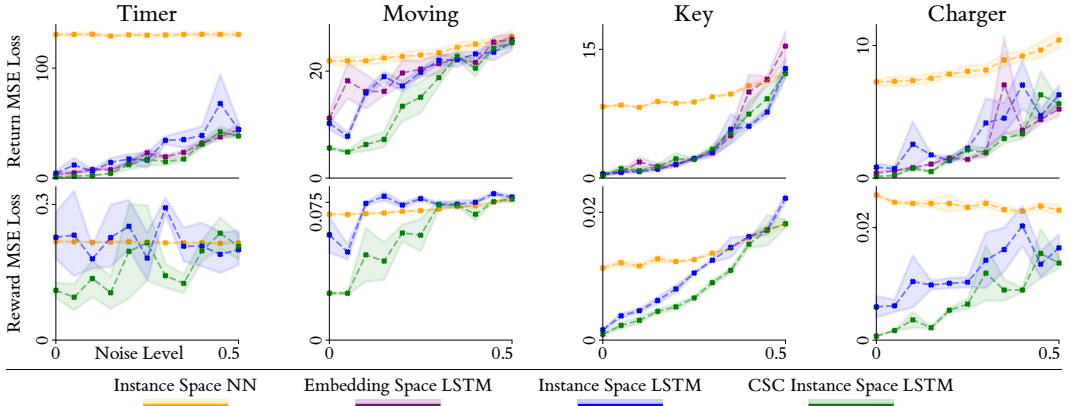


Figure 6: The return and reward performance of the MIL RM models (three repeats) subject to label noise. Note we omit the Embedding Space LSTM reward losses as they are very high.

metrics aside from Timer reward loss (where the mix of negative and positive rewards makes the effect of noise especially unpredictable), a noise level of at least 0.3 is required for the CSC Instance Space LSTM to perform as badly as the Instance Space NN baseline does with no noise at all.

5 Discussion

In this section, we seek to interpret our MIL RM models, analysing the distribution of learnt hidden states (Section 5.1) as well as their temporal dynamics over the course of a trajectory (Section 5.2). Finally, in Section 5.3 we discuss the limitations of this work and potential areas for future work.

5.1 Hidden State Analysis

The primary purpose of RM is to perform accurate reward reconstruction to facilitate agent training, but there is a secondary opportunity to improve understanding of human preferences through interpretability analysis of the learnt models. We can directly visualise the 2D LSTM hidden states of our oracle experiments, which enables a qualitative comparison of the interpretability of the various model architectures (see Figure 7). Visualising the hidden states with respect to the temporal dependencies indicates that the CSC Instance Space LSTM has learnt insightful hidden state representations. Breaking down the CSC Instance Space LSTM hidden embeddings: for the Timer task, time is represented along a curve, with a sparser representation around $t = 50$ (the crossover point when the treasure reward becomes positive). For the Moving task, time is similarly captured along with an additional notion of the change in treasure direction from right to left. For the Key task, the binary state of no key vs key is separated, with additional partitioning based on x position, denoting the two different start points of the agent. We discuss the Charger task in Section 5.2.

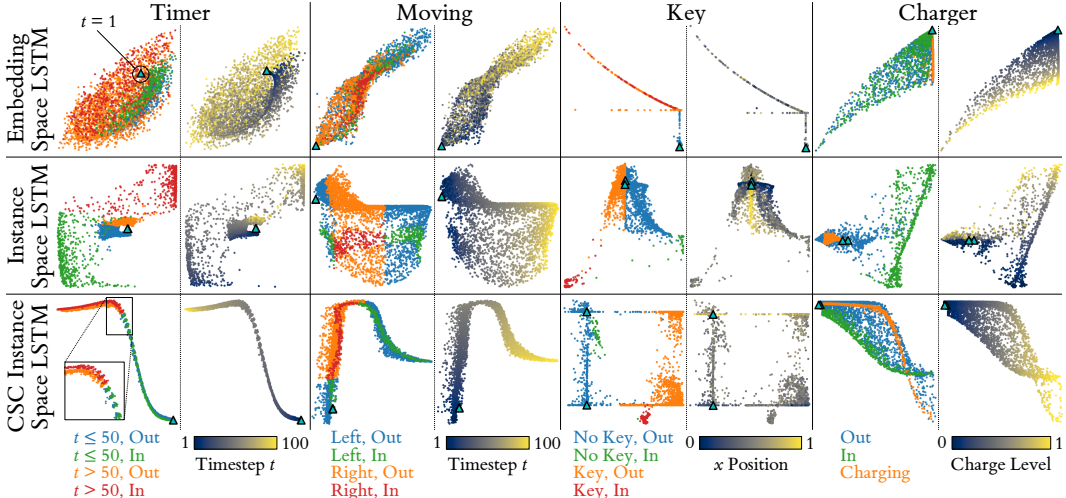


Figure 7: Learnt hidden state embeddings for our MIL RM models. For each model and task, we categorise the hidden state embeddings depending on the true environment state (first column for each task; In and Out indicate whether the agent is in the treasure or not; Left and Right indicate the direction in which the goal is currently moving). We also provide labelling based on temporal information (second column for each task). Furthermore, we include markers to indicate the hidden states for the centres of the agent spawn zones. For the Key task, as the temporal information is captured in the state categorisation (no key vs key), we use the second column to show the relationship between the hidden embeddings and the agent’s x position. This helps to showcase the separation of the two possible start spaces learnt by the CSC Instance Space LSTM model. We elected to use the best performing repeat for each model as assessed by the reward reconstruction (see Table 1).

5.2 Trajectory Probing

We further interpret our models by visualising the learnt reward with respect to the environment state, and by using hand-specified *probe* trajectories to verify that the learnt hidden state transitions mimic the true transitions. We present the above for the CSC Instance Space LSTM model on the Charger task in Figure 8 (Appendix F contains similar figures for the other tasks). The top row shows that the

model has correctly learnt the relationships between position, charge, and reward (reward increases only in the treasure zone as charge increases). From the probes, we can see how the charge level can be recovered from the hidden states. We also note that the inflection point between under-charging and over-charging is captured, i.e., this is where the optimal charge level lies, subject to some noise based on where the agent starts in the spawn zones. Furthermore, with the Challenging probe, we observe that the learnt hidden states align with the agent moving in and out of the charging zone.

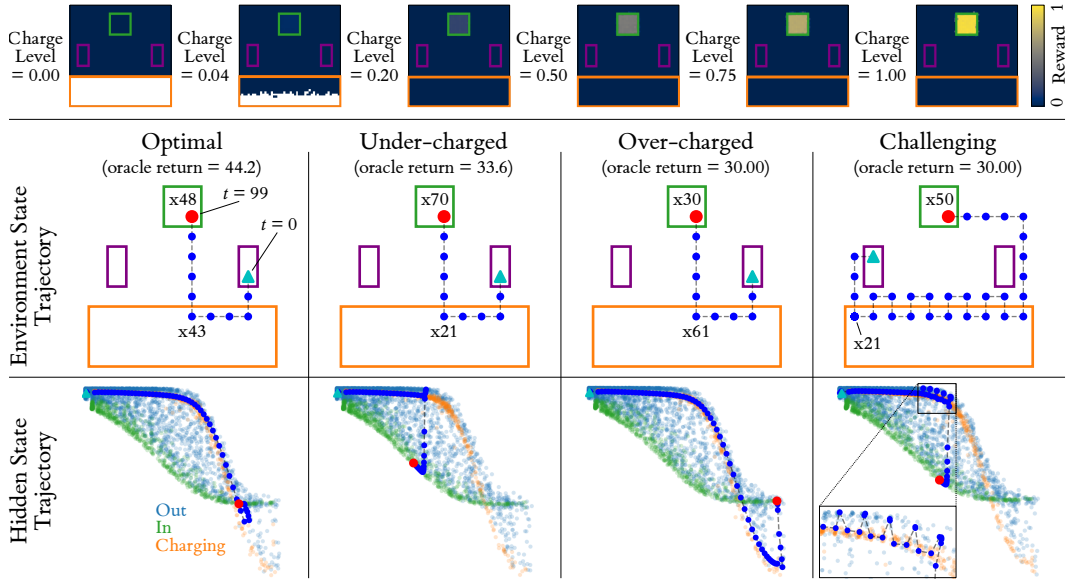


Figure 8: Interpretability for the CSC Instance Space LSTM on the Charger task. **Top:** the learnt relationship between agent position, charge level and reward. **Bottom:** Four probe trajectories demonstrating hidden state transitions as the trajectory progresses. *Optimal*: best possible return by charging to a sufficient level and maximising time in treasure. *Under-charged*: reward for treasure is too low. *Over-charged*: time is wasted charging after the maximum charge of 1 is reached. “ xn ” labels indicate the agent remaining in a position for n timesteps. As in Figure 7, this figure investigates the best performing model according to reward reconstruction.

5.3 Limitations and Future Work

Although we analyse the performance of our methods in the presence of noisy labels in Section 4.4, a major area of future work is to apply our methods to actual human data, potentially as a diagnostic tool to understand the extent to which real preferences are non-Markovian, and to generalise the learning to other information sources such as trajectory demonstrations [28] and pairwise choices [12]. Furthermore, we perform RM from an offline dataset before integrating fixed models into RL training; an iterative bootstrapping approach (learning from trajectories generated by the RL agent itself) is likely to be more practically useful. More generally, we hope that our identification of the link between RM and MIL may inspire a bidirectional transfer of tools and techniques.

6 Conclusion

We posed the problem of non-Markovian RM, which removes an unrealistic assumption about how humans evaluate temporally-extended agent behaviours. After identifying an isomorphism between RM and MIL, we proposed and evaluated novel MIL-inspired models that allow us to reconstruct non-Markovian reward functions, augment agent training, and interpret their learnt representations.

Acknowledgements

We would like to thank the University of Southampton, University of Bristol, and the Alan Turing Institute for their support. The authors acknowledge the use of the IRIDIS and BlueCrystal high performance computing facilities at Southampton and Bristol respectively, and associated support services at both universities, in the completion of this work.

References

- [1] D. Ariely and Z. Carmon. Gestalt characteristics of experiences: The defining features of summarized events. *Journal of Behavioral Decision Making*, 13(2):191–201, 2000.
- [2] F. Bacchus, C. Boutilier, and A. Grove. Rewarding behaviors. In *Proceedings of the National Conference on Artificial Intelligence*, pages 1160–1167, 1996.
- [3] F. Bacchus, C. Boutilier, and A. Grove. Structured solution methods for non-markovian decision processes. In *AAAI/IAAI*, pages 112–117. Citeseer, 1997.
- [4] A. Bajcsy, D. P. Losey, M. K. O’Malley, and A. D. Dragan. Learning robot objectives from physical human interaction. In *Conference on Robot Learning*, pages 217–226. PMLR, 2017.
- [5] B. Bakker. Reinforcement learning with Long Short-term Memory. *Advances in Neural Information Processing Systems*, 14, 2001.
- [6] C. Basu, E. Büyükkö, Z. He, M. Singhal, and D. Sadigh. Active learning of reward dynamics from hierarchical queries. In *2019 IEEE/RSJ International Conference on Intelligent Robots and Systems (IROS)*, pages 120–127. IEEE, 2019.
- [7] K. C. Berridge and J. P. O’Doherty. From experienced utility to decision utility. In *Neuroeconomics*, pages 335–351. Elsevier, 2014.
- [8] T. Bewley and F. Lecue. Interpretable Preference-based Reinforcement Learning with Tree-Structured Reward Functions. In *21st International Conference on Autonomous Agents and Multiagent Systems*, 2022.
- [9] G. Brockman, V. Cheung, L. Pettersson, J. Schneider, J. Schulman, J. Tang, and W. Zaremba. Openai gym, 2016.
- [10] M.-A. Carbonneau, V. Cheplygina, E. Granger, and G. Gagnon. Multiple instance learning: A survey of problem characteristics and applications. *Pattern Recognition*, 77:329–353, 2018.
- [11] L. Chan, A. Critch, and A. Dragan. The impacts of known and unknown demonstrator irrationality on reward inference. 2020.
- [12] P. F. Christiano, J. Leike, T. Brown, M. Martic, S. Legg, and D. Amodei. Deep reinforcement learning from human preferences. *Advances in Neural Information Processing Systems*, 30, 2017.
- [13] J. Early, C. Evers, and S. Ramchurn. Model Agnostic Interpretability for Multiple Instance Learning. In *International Conference on Learning Representations*, 2022.
- [14] M. Hausknecht and P. Stone. Deep Recurrent Q-learning for Partially Observable MDPs. In *2015 AAAI Fall Symposium Series*, 2015.
- [15] K. He, X. Zhang, S. Ren, and J. Sun. Deep residual learning for image recognition. In *Proceedings of the IEEE conference on computer vision and pattern recognition*, pages 770–778, 2016.
- [16] S. Hochreiter and J. Schmidhuber. Long short-term memory. *Neural computation*, 9(8):1735–1780, 1997.
- [17] G. Huang, Z. Liu, L. Van Der Maaten, and K. Q. Weinberger. Densely connected convolutional networks. In *Proceedings of the IEEE conference on computer vision and pattern recognition*, pages 4700–4708, 2017.
- [18] R. T. Icarte, T. Klassen, R. Valenzano, and S. McIlraith. Using reward machines for high-level task specification and decomposition in reinforcement learning. In *International Conference on Machine Learning*, pages 2107–2116. PMLR, 2018.
- [19] M. Ilse, J. Tomczak, and M. Welling. Attention-based deep multiple instance learning. In *International conference on machine learning*, pages 2127–2136. PMLR, 2018.
- [20] F. Jarboui and V. Perchet. Trajectory representation learning for multi-task nmrpd planning. In *2020 25th International Conference on Pattern Recognition (ICPR)*, pages 6786–6793. IEEE, 2021.
- [21] H. J. Jeon, S. Milli, and A. Dragan. Reward-rational (implicit) choice: A unifying formalism for reward learning. *Advances in Neural Information Processing Systems*, 33:4415–4426, 2020.
- [22] L. P. Kaelbling, M. L. Littman, and A. R. Cassandra. Planning and acting in partially observable stochastic domains. *Artificial intelligence*, 101(1-2):99–134, 1998.
- [23] D. Kahneman. Evaluation by moments: Past and future. *Choices, values, and frames*, pages 693–708, 2000.

[24] K. Lee, L. Smith, A. Dragan, and P. Abbeel. B-pref: Benchmarking preference-based reinforcement learning. In *Thirty-fifth Conference on Neural Information Processing Systems Datasets and Benchmarks Track*, 2021.

[25] J. Leike, D. Krueger, T. Everitt, M. Martic, V. Maini, and S. Legg. Scalable agent alignment via reward modeling: a research direction. *arXiv preprint arXiv:1811.07871*, 2018.

[26] D. Li and Y. Zhang. Multi-instance learning algorithm based on lstm for chinese painting image classification. *IEEE Access*, 8:179336–179345, 2020.

[27] V. Mnih, K. Kavukcuoglu, D. Silver, A. A. Rusu, J. Veness, M. G. Bellemare, A. Graves, M. Riedmiller, A. K. Fidjeland, G. Ostrovski, et al. Human-level control through deep reinforcement learning. *nature*, 518(7540):529–533, 2015.

[28] A. Y. Ng, S. J. Russell, et al. Algorithms for inverse reinforcement learning. In *International Conference on Machine Learning*, volume 1, page 2. PMLR, 2000.

[29] S. Reddy, A. Dragan, S. Levine, S. Legg, and J. Leike. Learning human objectives by evaluating hypothetical behavior. In *International Conference on Machine Learning*, pages 8020–8029. PMLR, 2020.

[30] D. Rolnick, A. Veit, S. Belongie, and N. Shavit. Deep learning is robust to massive label noise. *arXiv preprint arXiv:1705.10694*, 2017.

[31] S. Russell. *Human Compatible: Artificial Intelligence and the Problem of Control*. Penguin, 2019.

[32] A. Shah, S. Wadhwania, and J. Shah. Interactive robot training for non-markov tasks. *arXiv preprint arXiv:2003.02232*, 2020.

[33] Z. Shao, H. Bian, Y. Chen, Y. Wang, J. Zhang, X. Ji, et al. Transmil: Transformer based correlated multiple instance learning for whole slide image classification. *Advances in Neural Information Processing Systems*, 34, 2021.

[34] K. E. Stanovich. Higher-order preferences and the master rationality motive. *Thinking & Reasoning*, 14(1):111–127, 2008.

[35] S. Thiébaut, C. Gretton, J. Slaney, D. Price, and F. Kabanza. Decision-theoretic planning with non-markovian rewards. *Journal of Artificial Intelligence Research*, 25:17–74, 2006.

[36] J. Tien, J. Z.-Y. He, Z. Erickson, A. D. Dragan, and D. Brown. A study of causal confusion in preference-based reward learning. *arXiv preprint arXiv:2204.06601*, 2022.

[37] R. Toro Icarte, E. Waldie, T. Klassen, R. Valenzano, M. Castro, and S. McIlraith. Learning reward machines for partially observable reinforcement learning. *Advances in neural information processing systems*, 32, 2019.

[38] M. Tu, J. Huang, X. He, and B. Zhou. Multiple instance learning with graph neural networks. *arXiv preprint arXiv:1906.04881*, 2019.

[39] H. Van Hasselt, A. Guez, and D. Silver. Deep reinforcement learning with double q-learning. In *Proceedings of the AAAI conference on artificial intelligence*, volume 30, 2016.

[40] K. Wang, J. Oramas, and T. Tuytelaars. In defense of lstms for addressing multiple instance learning problems. In *Proceedings of the Asian Conference on Computer Vision*, 2020.

[41] X. Wang, Y. Yan, P. Tang, X. Bai, and W. Liu. Revisiting multiple instance neural networks. *Pattern Recognition*, 74:15–24, 2018.

[42] D. Wierstra, A. Förster, J. Peters, and J. Schmidhuber. Recurrent policy gradients. *Logic Journal of the IGPL*, 18(5):620–634, 2010.

A Implementation and Resource Details

This work was implemented in Python 3.8 and the machine learning functionality used PyTorch. All required libraries for our work are given in a `requirements.txt` file. Our code is included in the Supplementary Material submission and will be made publicly accessible once the work is published. The majority of MIL model training was carried out on a remote GPU service using a Volta V100 Enterprise Compute GPU with 16GB of VRAM, which utilised CUDA v11.0 to enable GPU support (IRIDIS 5, University of Southampton). Training each MIL model took a maximum of two hours (although we trained ten MIL models for each dataset with different dataset splits). Trained models are included alongside the code. Fixed seeds were used to ensure consistency of dataset splits between training and testing; these are included in the scripts that are used to run the experiments. All our datasets were generated from code; both the scripts to generate the data and also the derived datasets themselves are included alongside our model training code. Dataset generation, as well as all RL agent training, was conducted on a second remote GPU service using a compute node with two Nvidia Pascal P100 cards (BlueCrystal Phase 4, University of Bristol). Data generation took a maximum of three hours per dataset. Agent training was computationally light, requiring 8-12 minutes per 400-episode run, although we completed ten repeat runs for each permutation of task and MIL model architecture (one per MIL training repeat). Further details on executing the scripts to reproduce our results can be found in the `README.md` file in our code submission.

B Use Cases for Non-Markovian Reward Modelling

The non-Markovian reward formulation applies to cases where rewards depend on hidden state information h_t in addition to environment states s_t and actions a_t , and this information is a function of previous state-action pairs but *not* vice versa (i.e., there is no causal path from h_t to s_{t+k} for any $k > 1$). This crucial caveat distinguishes the formulation from the more general class of partially observable MDPs and demarcates the set of domains to which it can be applied: those involving a secondary Markovian system that “spectates” on events in the environment without intervening. In the RM context, this secondary system is a black box (making its internal state h_t hidden) and explicit rewards are unavailable, being replaced by sparser and potentially noisy form of reward-dependent feedback (trajectory return labels in our work). Below we identify three classes of use case which fit this technical specification and provide one concrete example for each:

Ambiguous Subtasks Cases involving an extended task with a sequential structure, where it is hard to formally define the conditions for subtask completion, but RM is feasible because a human “knows it when they see it”. Here, the hidden state to be learnt represents the current subtask and any auxiliary information needed to determine its completion status.

- **Concrete Example:** Using judges’ scores to learn a performative display (e.g., gymnastics, aerobatics) chaining several manoeuvres whose start and end conditions are difficult to formalise *a priori*. This could be considered as an extension of the single backflip task studied in the foundational RM work by Christiano et al. [12].

Dependencies on Subjective Affect Cases where a human’s reward function is dependent on their affective (emotional) status, which in turn depends on their prior experiences. Assuming this information is not directly available from the observed environment state, it must be learnt from data.

- **Concrete Example:** Using periodic satisfaction ratings to train a personal assistant robot whose owner’s mood, needs and preferences vary from day to day. These variations may influence the preferred driving style of a chauffeur service or choice of evening meal.

Irrationalities/Cognitive Biases Cases where one or more forms of bias colour a human’s post hoc rating of an observed trajectory, even if their instantaneously-experienced reward is Markovian. Psychological studies of how humans aggregate immediate rewards into retrospective evaluations of the quality of an experience find that a straight summation assumption is unrealistic, with subjects exhibiting high sensitivity to contrast effects and recency bias (collectively termed the peak-end rule)

[23], and factoring in anticipated future states in addition to those actually observed [1]. Here, the hidden state captures an aggregate representation of the biases at play in a given human’s evaluation.⁴

- **Concrete Example:** Using customer “star ratings” to improve a holiday planning agent whose recommendations aim to account for an unknown mix of biases such as the peak-end rule. The agent may use the learnt bias model to prioritise key moments in a holiday when managing the travel schedule and budget, in order to maximise future customers’ star ratings.

Finally, we note that it is a matter of taste as to whether hidden state information is framed as situated *inside a human evaluator’s mind* or *in the environment but only visible to the human*. It is not technically necessary to decide between these two framings, as the mathematical problem of non-Markovian RM is equivalent. From an agent’s perspective, a human evaluator is part of an augmented environment, even if they never intervene directly to influence the state.

C Preliminary Experiments on Toy Datasets

In this section, we give detail our preliminary experiments that were run on toy problems to initially develop and validate our approach. Below we outline the datasets (Section C.1), models and training hyperparameters (Section C.2), and results (Section C.3) of these experiments.

C.1 Datasets

We introduce three toy datasets, each abstracted from the RL context, to act as benchmark tests for our models. Each of these datasets uses ordered bags comprised of two-dimensional instances, where each instance has an associated label (called “reward” below, for consistency), and the overall bag label (return) is the sum of the instance labels.

Toggle Switch An instance is the position of a toggle switch ts and a value v ; if the switch is on ($ts = 1$), then the reward for the instance is v ; otherwise the reward for the instance is 0. Here, there is no hidden information, as it is possible to calculate the reward for an instance from its contents ts, v alone. This serves as a null example to elucidate what happens in a Markovian setting.

Push Switch We modify the toggle switch setup so that the instance now represents a push switch ($p = 1$ if this switch is pressed), where pressing the switch flips a binary hidden state ts (the same information as was previously represented by the toggle switch). This hidden state then determines the reward as before (v if $ts = 0$, else 0). As ts must be tracked between successive instances, it is not possible to determine the reward for an instance solely by observing its contents p, v , so this setup is non-Markovian.

Dial We generalise the hidden state from a binary switch to a continuous-valued dial. Given an instance m, v , the dial’s current value d is moved up or down by m . The reward is then given as $d \cdot v$. The problem remains non-Markovian, but now the hidden state that needs tracking, d , is continuous rather than discrete.

C.2 Models and Hyperparameters

When training the MIL models on the toy dataset, we used the Adam optimiser with a batch size of one (i.e., one bag per batch) to minimise mean squared error (MSE) loss. Training was performed using validation loss early stopping, i.e., if the validation loss did not decrease after a certain number

⁴A fascinating philosophical question arises here. When (following the method of Section 3.3) an RL agent is trained using a non-Markovian RM model that captures a cognitive bias, should the agent learn to maximise rewards *including* the bias (which, for example, might lead it to prioritise its peak and final reward rather than seek uniformly good performance), or *excluding* it (which would revert to uniform prioritisation). This issue of whether intelligent agents should seek to exploit human irrationalities when optimising for their revealed preferences, or appeal to their unbiased “better angels”, relates to distinctions between first- and second-order preferences [34] or between experienced and remembered (or decision) utility [7]. We defer this question to those with more relevant expertise but note that regardless of the answer, it is essential to include the biases in the reward model using a method such as the one proposed in this work.

of training epochs (patience value), we terminated the training and selected the model at which the validation loss was lowest. If the patience value was not reached (i.e., the validation loss kept decreasing), we terminated training after a maximum number of epochs had been reached, and again selected the model at which the validation loss was lowest. The hyperparameters for training the models on each dataset (including learning rate (LR) and weight decay (WD)) are given in Table A1. Dropout was not used. These hyperparameters were found through a small amount of trial and error, i.e., no formal hyperparameter tuning was carried out.

Table A1: Toy dataset training hyperparameters.

Dataset	LR	WD	Patience	Epochs
Toggle Switch	1×10^{-4}	1×10^{-5}	20	100
Push Switch	1×10^{-3}	0	30	150
Dial	1×10^{-3}	0	30	150

In Tables A2 to A5 we give the architectures for the MIL models we used in the toy dataset experiments. The models are a combination of fully connected layers (FC) along with different MIL pooling mechanisms. Some layers also include rectified linear unit (ReLU) activation. We label the layers based on the part of the network they belong to: feature extractor (FE), head network (HN), or pooling (P); see Section 3.2. We also indicate the input and output sizes: $b \times n$ indicates an input or output where there is a representation of length n for each of the b instances (b is the size of the input bag).

Table A2: Toy Instance Space NN

Layer	Type	Input	Output
1 (FE)	FC + ReLU	$b \times 2$	$b \times 2$
2 (HN)	FC	$b \times 2$	$b \times 1$
3 (P)	mil-sum	$b \times 1$	1

Table A3: Toy Embedding Space LSTM

Layer	Type	Input	Output
1 (FE)	FC + ReLU	$b \times 2$	$b \times 2$
2 (P)	mil-emb-lstm	$b \times 2$	2
3 (HN)	FC	2	1

Table A4: Toy Instance Space LSTM

Layer	Type	Input	Output
1 (FE)	FC + ReLU	$b \times 2$	$b \times 2$
2 (P-1)	mil-ins-lstm	$b \times 2$	$b \times 2$
3 (HN)	FC	$b \times 2$	$b \times 1$
4 (P-2)	mil-sum	$b \times 1$	1

Table A5: Toy CSC Instance Space LSTM

Layer	Type	Input	Output
1 (FE)	FC + ReLU	$b \times 2$	$b \times 2$
2 (P-1)	mil-csc-ins-lstm	$b \times 2$	$b \times 2$
3 (HN)	FC	$b \times 2$	$b \times 1$
4 (P-2)	mil-sum	$b \times 1$	1

C.3 Results

For each of the toy datasets, we generate 5000 random bags with between 10 and 20 instances per bag (uniformly distributed). We use an 80/10/10 dataset split for training, validation, and testing, and repeat our experiments with ten different variations of this split (so in total we have ten repeats of each model type for each dataset). We show results for both return and reward reconstruction for the toy datasets in Table A6. From these results, we can make several observations. Firstly, as expected, the Instance Space NN architecture only works on the Markovian Toggle Switch dataset, i.e., it fails on the non-Markovian Push Switch and Dial datasets as it is unable to deal with temporal dependencies. We also note that our two proposed architectures (Instance Space LSTM and CSC Instance Space LSTM) outperform the baseline Embedding Space LSTM method on both return and reward, with the CSC Instance Space LSTM providing the best results overall. Finally, we observe that a better return performance does not always guarantee better reward performance: for the Dial dataset, the Instance Space LSTM makes better return predictions than the CSC Instance Space LSTM, but worse reward predictions. A similar outcome can be seen for the Embedding Space LSTM and the Instance Space NN on the Push Switch dataset.

Table A6: Toy dataset return (top) and reward (bottom) results. Each measurement is the mean MSE averaged over ten repeats, with the standard errors of the mean also given. Bold entries indicate the best performing model for each (metric, dataset) pair.

Model	Toggle Switch	Push Switch	Dial	Overall
Instance Space NN	0.030 ± 0.029	3.337 ± 0.054	5.489 ± 0.157	2.952
Embedding Space LSTM	0.008 ± 0.002	0.663 ± 0.194	0.434 ± 0.075	0.368
Instance Space LSTM	0.062 ± 0.058	0.262 ± 0.154	0.111 ± 0.014	0.145
CSC Instance Space LSTM	0.000 ± 0.000	0.140 ± 0.065	0.121 ± 0.043	0.087
Instance Space NN	0.002 ± 0.002	0.086 ± 0.001	0.954 ± 0.011	0.347
Embedding Space LSTM	0.003 ± 0.001	0.206 ± 0.100	0.244 ± 0.077	0.151
Instance Space LSTM	0.004 ± 0.004	0.021 ± 0.008	0.026 ± 0.004	0.017
CSC Instance Space LSTM	0.000 ± 0.000	0.012 ± 0.004	0.022 ± 0.007	0.011

D RL Task Details, Data Generation and Model Hyperparameters

In this section, we give more detail on the reward reconstruction experiments for the RL tasks. First, we give more information about the RL tasks (Section D.1), then explain how we generated datasets from the tasks (Section D.2), and finally we give the MIL model architectures and hyperparameters used for these experiments (Section D.3).

D.1 Task Details

All four of our experimental RL tasks are implemented in Python within a common 2D simulator following the OpenAI Gym standard [9]. The agent’s position x, y is moved by one of five discrete actions: up, down, left, right and no-op. In the first four cases, the position is moved by 0.1 in the specified direction. The motion vector is then corrupted by zero-mean Gaussian noise with a standard deviation of 0.02 in both x and y and clipped into the bounds $[0, 1]^2$. Zones of interest (spawn zones, treasure, key, charger) are specified as rectangles lying within these bounds. At time t , the environment state s_t (which is directly observed by the MIL RM models) is the 2D vector of the current position $[x_t, y_t]$; its dynamics are Markovian given the agent’s chosen action. The hidden state h_t is the task-specific information that renders the oracle’s reward function R Markovian:

- **Timer:** $h_0 = 0$ and $h_{t+1} = \delta(h_t, s_t, a_t) = h_t + 1$; the hidden state simply tracks the current timestep index. Reward is given by⁵

$$R(s_t, a_t, h_{t+1}) = \text{in_treasure}(s_t) \cdot \begin{cases} -1 & \text{if } h_{t+1} \leq 50, \\ +1 & \text{otherwise,} \end{cases}$$

where $\text{in_treasure}(s_t) = 1$ if $0.4 \leq s_t^0 \leq 0.6$ and $0.7 \leq s_t^1 \leq 0.9$, and 0 otherwise (note that $s_t^0 = x_t, s_t^1 = y_t$).

- **Moving:** $h_0 = [0.4, -0.02]$, the initial horizontal position (left edge) and velocity of the moving treasure rectangle. Hidden state dynamics encode the left-right oscillation:

$$h_{t+1} = \delta(h_t, s_t, a_t) = \left[h_t^0 + h_t^1, \begin{cases} h_t^1 & \text{if } 0 < (h_t^0 + h_t^1) < 0.8, \\ -h_t^1 & \text{otherwise} \end{cases} \right].$$

Reward is given by $R(s_t, a_t, h_{t+1}) = 1$ if $h_{t+1} \leq s_t^0 \leq (h_{t+1} + 0.2)$ and $0.7 \leq s_t^1 \leq 0.9$, and 0 otherwise.

- **Key:** $h_0 = 0$, indicating that the agent initialises without the key. The key collection dynamics are encoded by

$$h_{t+1} = \begin{cases} 1 & \text{if } 0.4 \leq s_t^0 \leq 0.6 \text{ and } 0.1 \leq s_t^1 \leq 0.3, \\ h_t & \text{otherwise.} \end{cases}$$

Reward is given by $R(s_t, a_t, h_{t+1}) = \text{in_treasure}(s_t) \cdot h_{t+1}$, where the in_treasure function is the same as in the Timer task.

⁵Note the timestep indices used here, which result from the order in which environment states, hidden states and rewards are computed. At time t , the hidden state h_t is first updated to h_{t+1} by $\delta(h_t, s_t, a_t)$, then the reward is computed as $R(s_t, a_t, h_{t+1})$, and finally the environment state is updated to s_{t+1} by $D(s_t, a_t)$.

- **Charger:** $h_0 = 0$, indicating an initial charge level of zero. The charging dynamics are encoded by

$$h_{t+1} = \begin{cases} \min(h_t + 0.02, 1) & \text{if } s_t^1 \leq 0.3, \\ h_t & \text{otherwise.} \end{cases}$$

Reward is given identically to the Key task, $R(s_t, a_t, h_{t+1}) = \text{in_treasure}(s_t) \cdot h_{t+1}$.

D.2 MIL Dataset Generation

We obtain datasets of 5000 trajectories per task, containing a wide distribution of outcomes and return values, as follows. For each task k , we define a discrete *trajectory outcome* function $O_k : \Xi \rightarrow \mathcal{O}_k$ and a limit n_k on the number of trajectories that are allowed to map to any element of the outcome set \mathcal{O}_k . These are given as follows:

- **Timer:** $\mathcal{O}_{\text{timer}} = \text{num_neg} \times \text{num_pos}$, where $\text{num_neg} = \{0..50\}$ counts the number of timesteps the agent spends in the treasure while its reward is negative ($t \leq 50$), and $\text{num_pos} = \{0..50\}$ counts the number while the reward is positive ($t > 50$). The outcome set cardinality is $|\mathcal{O}_{\text{timer}}| = 51^2 = 2601$ and the per-outcome limit is $n_{\text{timer}} = 10$ trajectories.
- **Moving:** $\mathcal{O}_{\text{moving}} = \text{num_treasure}$, where $\text{num_treasure} = \{0..100\}$ counts the timesteps spent in the treasure. $|\mathcal{O}_{\text{moving}}| = 101$ and $n_{\text{moving}} = 250$.
- **Key:** $\mathcal{O}_{\text{key}} = \{\text{no_key}, \text{key_no_treasure}, \text{treasure}\}$, where the outcome is `no_key` if the key is not collected, `key_no_treasure` if the key is collected but the treasure is not reached, and `treasure` if the treasure is reached after collecting the key. $|\mathcal{O}_{\text{key}}| = 3$ and n_{key} is defined on a per-outcome basis: 1250 for `no_key` and `key`, and 2500 for `treasure`.
- **Charger:** $\mathcal{O}_{\text{charger}} = \text{num_treasure} \times \text{charge_bin}$, where $\text{num_treasure} = \{0..100\}$ counts the timesteps spent in the treasure and $\text{charge_bin} = \{1..20\}$ is a binned representation of the *mean* charge level when in the treasure (e.g. 0.0 maps to bin 1, 0.48 to bin 10, 0.96 to bin 20). $|\mathcal{O}_{\text{charger}}| = 2020$ and $n_{\text{charger}} = 10$.

The dataset for task k , \mathbf{X}_k , is assembled by an iterative algorithm. On each iteration, we generate a length-100 trajectory, ξ , by sampling agent actions uniform-randomly from the available set (up, down, left, right, no-op) and running them through the simulator. Once the trajectory is complete, we evaluate its outcome $O_k(\xi)$. If there are already at least n_k trajectories in \mathbf{X}_k with this outcome, ξ is discarded. Otherwise, it is added to \mathbf{X}_k . This process repeats until $|\mathbf{X}_k| = 5000$.

D.3 MIL Models and Hyperparameters

The MIL model training on the synthetic RL tasks used the same process as for the toy model training (see Section C.2). However, we also applied dropout (DO) in these models. We give the MIL training hyperparameters for each of the RL tasks in Table A7. Again, these hyperparameters were found through a small amount of trial and error, i.e., no formal hyperparameter tuning was carried out.

Table A7: Synthetic RL task MIL training hyperparameters.

Dataset	LR	WD	DO	Patience	Epochs
Timer	5×10^{-4}	0	0.1	50	250
Moving	5×10^{-4}	0	0.1	50	250
Key	5×10^{-4}	0	0.1	30	150
Charger	5×10^{-4}	0	0.1	50	250

In Tables A8 to A11 we give the architectures for the MIL models we used in the synthetic RL dataset experiments. As in the toy dataset experiments, the models are a combination of fully connected layers (FC) along with different MIL pooling mechanisms. Some layers also include with rectified linear unit (ReLU) activation. Again, we label the layers based on the part of the network they belong to: feature extractor (FE), head network (HN), or pooling (P); see Section 3.2. We also indicate the input and output sizes: $b \times n$ indicates an input or output where there is a representation of length n for each of the b instances (b is the size of the input bag).

Table A8: RL Instance Space NN

Layer	Type	Input	Output
1 (FE-1)	FC + ReLU + DO	$b \times 2$	$b \times 64$
2 (FE-2)	FC + ReLU + DO	$b \times 64$	$b \times 32$
3 (FE-3)	FC + ReLU + DO	$b \times 32$	$b \times 32$
4 (HN-1)	FC + ReLU + DO	$b \times 32$	$b \times 32$
5 (HN-2)	FC + ReLU + DO	$b \times 32$	$b \times 16$
6 (HN-3)	FC	$b \times 16$	$b \times 1$
7 (P)	mil-sum	$b \times 1$	1

Table A9: RL Embedding Space LSTM

Layer	Type	Input	Output
1 (FE-1)	FC + ReLU + DO	$b \times 2$	$b \times 64$
2 (FE-2)	FC + ReLU + DO	$b \times 64$	$b \times 32$
3 (FE-3)	FC + ReLU + DO	$b \times 32$	$b \times 32$
4 (P)	mil-emb-lstm	$b \times 32$	2
5 (HN-1)	FC + ReLU + DO	2	32
6 (HN-2)	FC + ReLU + DO	32	16
7 (HN-3)	FC	16	1

Table A10: RL Instance Space LSTM

Layer	Type	Input	Output
1 (FE-1)	FC + ReLU + DO	$b \times 2$	$b \times 64$
2 (FE-2)	FC + ReLU + DO	$b \times 64$	$b \times 32$
3 (FE-3)	FC + ReLU + DO	$b \times 32$	$b \times 32$
4 (P-1)	mil-ins-lstm	$b \times 32$	$b \times 2$
5 (HN-1)	FC + ReLU + DO	$b \times 32$	$b \times 32$
6 (HN-2)	FC + ReLU + DO	$b \times 32$	$b \times 16$
7 (HN-3)	FC	$b \times 16$	$b \times 1$
8 (P-2)	mil-sum	$b \times 1$	1

Table A11: RL CSC Instance Space LSTM

Layer	Type	Input	Output
1 (FE-1)	FC + ReLU + DO	$b \times 2$	$b \times 64$
2 (FE-2)	FC + ReLU + DO	$b \times 64$	$b \times 32$
3 (FE-3)	FC + ReLU + DO	$b \times 32$	$b \times 32$
4 (P-1)	mil-csc-ins-lstm	$b \times 32$	$b \times 2$
5 (HN-1)	FC + ReLU + DO	$b \times 32$	$b \times 32$
6 (HN-2)	FC + ReLU + DO	$b \times 32$	$b \times 16$
7 (HN-3)	FC	$b \times 16$	$b \times 1$
8 (P-2)	mil-sum	$b \times 1$	1

E Further Details on RL Agent Training

Adopting OpenAI Gym terminology [9], non-Markovian reward functions (both ground-truth oracles and learnt LSTM-based models) are implemented as wrappers on rewardless base environments. The role of a wrapper is to track the hidden state of either the oracle or the LSTM throughout an episode and use this to compute rewards to return to the agent. In the “Oracle (without hidden state)” baseline, we return the raw environment state (the 2D position $[x_t, y_t]$) to the agent unmodified. Otherwise, we concatenate the post-update hidden state h_{t+1} onto the end of the environment state, thereby expanding the state space from the agent’s perspective and making rewards Markovian.

This wrapper-based approach allows us to use a completely vanilla RL agent architecture. For the sake of simplicity, we use a DQN agent [27] with the double Q-learning trick [39] enabled. We use a value network with ReLU activation functions and three hidden layers of 256, 128 and 64 neurons respectively, which is updated on every timestep by sampling batches of size 128 from a replay buffer of capacity 50000. Bellman updates use a discount factor of $\gamma = 0.99$ and are implemented by the Adam optimiser with a learning rate of 0.001. The target network tracks the primary one by Polyak averaging of parameters with a coefficient of 0.005 per timestep. Action selection follows an ϵ -greedy policy, with ϵ linearly decayed from 1 to 0.05 over the first 200 episodes and held constant thereafter. For all tasks, we find that 400 training episodes are generally sufficient to obtain policy convergence.

F Interpretability Plots for Other RL Tasks

In this section we give the interpretability plots (like Figure 8) for the timer (Figure A1), moving (Figure A2), and key (Figure A3) tasks. As before, we analyse the best performing CSC Instance Space LSTM model for each task (according to the reward reconstruction metric).

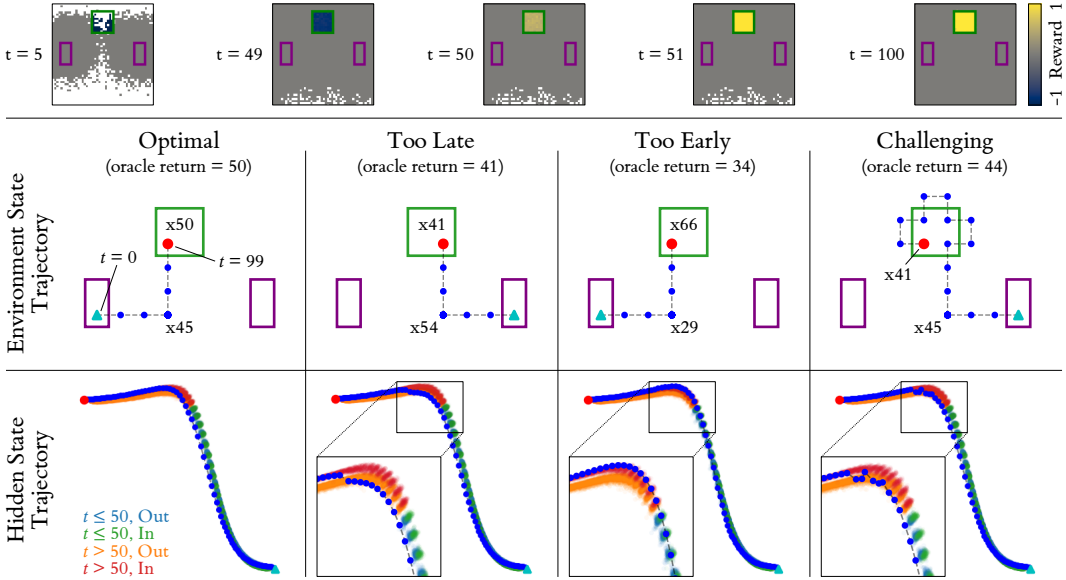


Figure A1: Key task interpretability.

Top: Predicted reward with respect to time and position. We observe that the model has correctly captured the transition from negative to positive reward in the treasure region at $t = 50$, with no reward outside of this region. Although the reward is positive at $t = 50$, the model is uncertain at this point, i.e., the transition from negative to positive reward happens over two timesteps rather than one. **Bottom:** Four interpretability probes demonstrating the model’s hidden state transitions. “ xn ” labels indicate the agent remaining in a position for n timesteps.

Optimal: The agent moves into the treasure region at $t = 50$ and remains there, receiving the maximum possible reward.

Too Late: The agent moves into the treasure region a while after the treasure has already become positive, i.e., it is missing out on reward by not being in the region for as long as possible. This is reflected in the hidden state plot, where the state transitions from the orange to the red region after the $t = 50$ boundary.

Too Early: The agent moves into the treasure region before the treasure becomes positive, therefore, while it earns the maximum amount of positive reward, it also earns negative reward, leading to a sub-optimal result.

Challenging: The agent moves into the treasure region at the correct time, but proceeds to jump in and out of the treasure region before settling, leading to lost reward. The hidden state trajectories somewhat mimic this movement by transitioning between the orange and red regions, although the jumps are less clear near to the $t = 50$ transition point, suggesting the model is uncertain at this point.

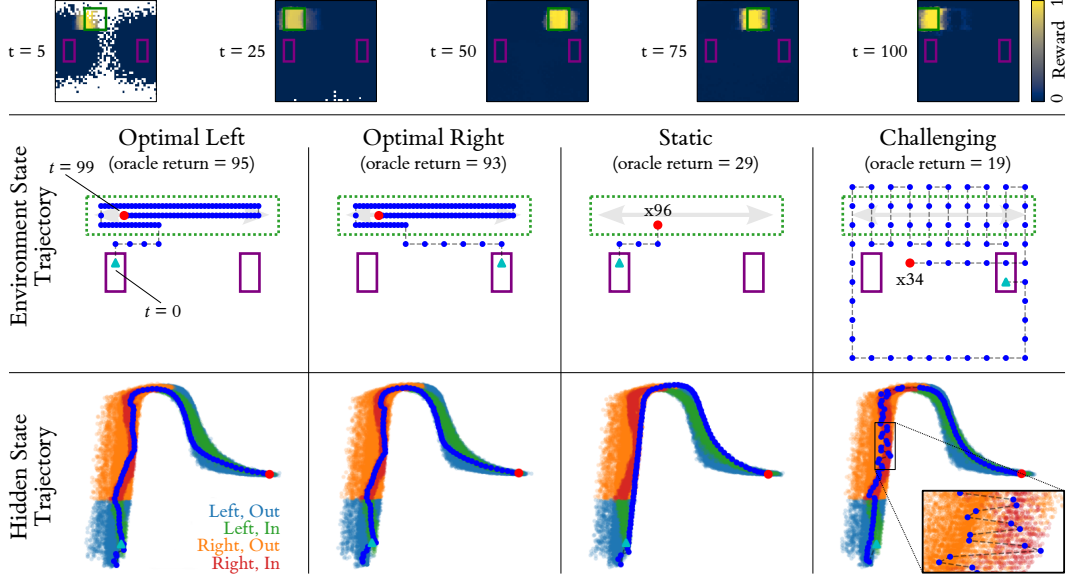


Figure A2: Moving task interpretability.

Top: The predicted reward with respect to time (and as such, position of the treasure region). The model has learnt to track the treasure region as it moves, although there is noise around the left and right edges of the region, highlighting the difficulty in tracking the treasure region's horizontal position.

Bottom: Four interpretability probes showing the model's hidden state transitions. Note the green dotted region indicates the overall boundary of the treasure region, i.e., the treasure lies somewhere within that boundary, with its true horizontal position dependent on time. “ xn ” labels indicate the agent remaining in a position for n timesteps.

Optimal Left: The agent moves within the treasure region as quickly as possible and then moves with the treasure (keeping within it) for the remainder of the episode. The hidden state trajectories follow the “In” regions (green and red).

Optimal Right: A similar optimal probe where the agent starts from the right-hand spawn zone rather than the left. In this case, the agent has further to move before moving into the treasure region, leading to slightly less overall reward than when it starts from the left.

Static: Rather than moving with the treasure region, the agent stays still and allows the treasure to pass over it, gaining reward for some timesteps but not others. We observe that the hidden state trajectory also reflects this — the state transitions between the “In” and “Out” regions.

Challenging: The agent takes a while to move towards the treasure region, and then passes in and out of the boundary in which the treasure resides, picking up some reward. We can see from the hidden state trajectory that this motion is captured in the hidden states — the trajectory transitions between the orange and red regions as the agent passes back and forth through the treasure region.

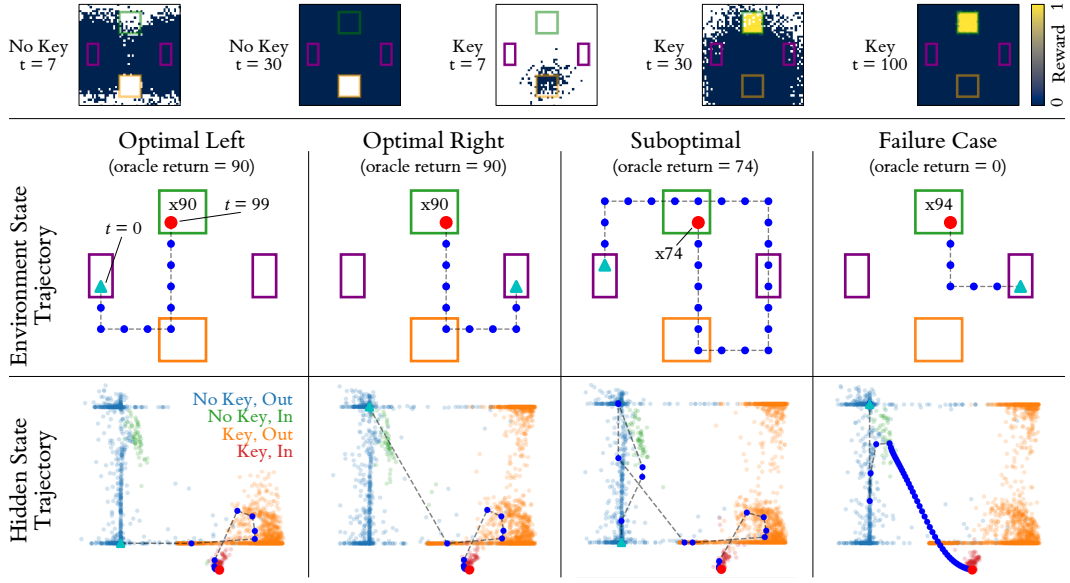


Figure A3: Key task interpretability.

Top: The predicted reward with respect to time and collection of the key. The model has learnt to only give reward when the agent is in the treasure region after collecting the key.

Bottom: Four interpretability probes showing the model’s hidden state transitions. “ xn ” labels indicate the agent remaining in a position for n timesteps.

Optimal Left: The agent collects the key as quickly as possible, and then proceeds to move into the treasure region and wait there until the end of the episode. The hidden state trajectory shows two notable transitions, first when the key is collected (blue to orange) and then when the agent enters the treasure region (orange to red).

Optimal Right: A similar optimal policy, but from the right-hand spawn zone rather than the left. Note the hidden state trajectory is very similar, apart from the initial hidden state, which is at the opposite side of the blue region, representing the different spawn position.

Suboptimal: The agent passes through the treasure region before collecting the key, and then follows an optimal policy. We observe a transition in the hidden state trajectory from the blue to the green region that corresponds to the agent’s premature entrance into the treasure region.

Failure case: The agent enters the treasure region without collecting the key and remains there for the rest of the episode. This highlights a failure case of the model, where the hidden state “drifts” from the green region to the red region, i.e., the model convinces itself that the agent must have picked up the key at some point. Such *causal confusion* errors are well-documented in the RM literature [36]. In our case, we suspect that the error is due to a bias in our data generation method inducing a correlation between key possession and time spent in the treasure region. As described in Appendix D.2, we specifically screen for trajectories where the treasure is visited with the key (the “treasure” outcome) but not for those where it is visited without it. There are thus likely to be very few training trajectories that spend a lot of time in the treasure region without collecting the key, making this probe an extreme outlier on which performance is poor. Adding and selecting for a fourth “key_no_treasure” outcome during data generation may have mitigated this issue.